Heterogeneous Interaction and Reaction of HONO on Ice Films between 173 and 230 K

Liang Chu, Guowang Diao, and Liang T. Chu*

Department of Environmental Health and Toxicology, State University of New York at Albany and Wadsworth Center, P.O. Box 509, Albany, New York 12201-0509

Received: October 18, 1999; In Final Form: January 11, 2000

Both the heterogeneous interaction of HONO on the ice surface and the heterogeneous reaction of HONO with HBr on the ice surface have been investigated in a flow reactor interfaced with a differentially pumped quadrupole mass spectrometer. The surface uptake amount and initial uptake coefficient of HONO on the ice surface were determined as a function of the ice-film temperature between 173 and 205 K. The reaction probability of HONO over the HBr-treated ice surfaces has been determined as a function of HBr partial pressures at 190K, 200K, and 230K, respectively. The reaction mechanism is proposed and discussed. Kinetic analysis indicates that the heterogeneous reaction of HONO with HBr on ice surfaces follows the Eley−Rideal type.

I. Introduction

Nitrous acid is an important trace gas in the troposphere. The gas-phase chemistry of HONO plays a role in the formation of hydroxyl radicals (OH) because HONO photolyzes rapidly to produce OH.[1,2] Because of its rapid photolysis at daytime, elevated concentrations of HONO have normally been observed only at night ranging from a few ppbv at polluted sites to 70 pptv in the Arctic.[3,4] Recent observations reveal that daytime steady-state HONO concentrations of 100−500 pptv have been observed in the clean troposphere.[2,5]

The atmospheric chemistry of bromine species is characterized by their short lifetimes and their ready availability for gas-phase catalytic cycles in the stratosphere.[6−8] The longest-lived reactive bromine species is HBr, but it constitutes only a small fraction of the total reactive bromine present in the atmosphere.[9] Even though it has a low concentration, HBr could be accumulated on the ice surface.[10−13] Heterogeneous bromine reactions play a role in converting bromine reservoir compounds, $BrONO_2$ and HBr, into photochemically reactive species.[9] The heterogeneous reaction of HBr on ice surfaces is limited to a few studies. Chu and Chu studied the heterogeneous reaction of HOCl + HBr on ice films.[14] Abbatt[10] and Allanic et al.[15] studied the heterogeneous reaction of HOBr + HBr on ice films. Hanson and Ravishankara investigated the heterogeneous reactions of $ClONO_2$ + HBr and Cl_2 + HBr on ice films.[13] With the higher HONO concentration in the troposphere and bromine reservoir HBr, it is reasonable to speculate that HONO may react with HBr on the ice surface. Recently, Seisel and Rossi demonstrated the feasibility of this reaction.[16]

Seisel and Rossi studied the reaction of HONO + HBr in the temperature range between 180 and 200 K and reported the reaction probability to be 1.0×10^{-3} to 2.2×10^{-2}, with almost no temperature dependence.[16] The rate of the reaction may be slightly accelerated by increasing HBr concentration. However, little is known about the mechanism of this reaction. From a fundamental surface chemistry standpoint, it is important to know which reactants adsorb on the ice surface and how molecules react each other on the ice surface. HBr may potentially form hydrate(s) near the ice surface at 190 and 200K in the fast-flow reactor.[11] At 230 K, HBr could possibly be in a liquid phase, according to the HBr phase diagram.[12] What is the difference in reaction mechanisms at 190 and 200K versus at 230K? Also, for the purpose of atmospheric chemistry, a reliable rate constant at atmospheric conditions provides a useful tool to model complex atmospheric reactions. A reliable heterogeneous reaction probability under atmospheric conditions can be extrapolated from the mechanistic studies. The heterogeneous reaction of HONO + HBr may play a role in the activation of bromine in the troposphere. This motivated us to study the reaction of HONO + HBr(s) → BrNO + H_2O(s) on ice surfaces.

In this paper, we report the results of our experiments on the uptake amount, uptake coefficient of HONO on the ice surface, and the reaction probability for the reaction of HONO + HBr(s) → BrNO + H_2O(s) on ice surfaces. In the following sections, we will briefly describe the experimental procedures used in the determination of the uptake amount, the uptake coefficient, and the reaction probability. We will present the results of the uptake amount and uptake coefficient of HONO on the ice surface as a function of ice-film temperatures. The reaction probability of the HONO + HBr reaction is a function of partial HBr pressures and ice-film temperatures. Finally, we will discuss the nature of the interaction between HONO and ice, and a reaction mechanism for the HONO + HBr reaction will be proposed.

II. Experimental Section

The uptake coefficient is defined as the ratio of the number of molecules that are taken by the surface to the total number of molecules colliding on the ice surface. Three different experiments, the uptake amount, uptake coefficient of HONO on the ice surface, and the reaction probability of HONO + HBr on the ice surface, were performed in a flow reactor coupled to a differentially pumped quadrupole mass spectrometer (QMS). Some of the apparatus details have been discussed in our previous publications,[11,14,17] and we provide only a brief description and some modifications in this paper.

* To whom correspondence should be addressed. e-mail: lchu@csc.albany.edu.

10.1021/jp9937151 CCC: $19.00
Published on Web 03/22/2000

Flow Reactor. The cylindrical flow reactor was constructed of Pyrex glass. Its dimensions were 1.70 cm i.d. and 35 cm in length. The temperature of the reactor was regulated by a liquid nitrogen-cooled ethanol circulator (Neslab), and was measured with a pair of J-type thermocouples located in the middle and at the downstream end. During the experiment, the temperature was maintained at 173, 180, 190, 200, and 230 K, and the stability of the temperature was better than 0.3 K in every experiment. The pressure of the reactor was controlled by a downstream throttle valve (MKS Instrument, Model 651C), and the stability of the pressure was better than 0.001 Torr in every experiment. A double-capillary injector was used to admit both HONO and HBr into the flow reactor during the reaction probability measurement. The reactant HONO vapor was taken from a nitrous acid solution. HONO vapor contains a small amount of water vapor. To avoid the condensation of the water vapor and reactants on the capillary wall at low temperatures, room-temperature dry air was passed through the outside of the capillary to keep it warm.

Ice-Film Preparation. The ice film was prepared as follows: Helium carrier gas was bubbled through a distilled-water reservoir. Deionized water was purified with a Millipore Mili-Q water system. The purified, distilled water had a resistivity ≥ 18 MΩ·cm and was used in the reservoir. The reservoir was maintained at 293.2 ± 0.1 K by a refrigerated circulator (Neslab RTE-100LP). Helium saturated with the water vapor was admitted to an inlet of the double-capillary injector. The ice film was separated into two sections. The first section was ~16.5 cm in length, and the second section was about 5 cm. The first section was used to conduct the experiments, and the second section, with extra thick ice (~0.1 mm), was used to keep the first section's ice film from being evaporated in the reactor. The two sections were separated by approximately 5−10 cm. Note that the reactants, HONO and HBr, made contact with the first section of the ice film only. During the course of ice deposition, the double-capillary injector was slowly pulled out at a constant rate, 2−3 cm/min, and a uniform ice film was deposited on the inner surface of the reactor, which was between 173 and 205 K. The amount of ice substrate deposited in the first section was determined from the mass flow rate of the water vapor and the deposition time. The average film thickness was calculated by using the measured ice film geometric area, the mass of the ice, and the bulk density, 0.63 g/cm^3, of vapor-deposited water ice.[18] The average film thickness was about 30 μm at 190 and 200 K. After the uniform ice film was deposited, the injector was rapidly moved to the second section, and the extra thick ice film was deposited near the end of flow tube. Because the injector and helium carrier gases could be a few degrees warmer than the ice film, they would heat the thick ice film at the end of flow tube. This provided a water vapor source that was always slightly higher than or equal to the ice vapor pressure at the ice film temperature in the flow reactor. This water vapor was supplied to the first section of ice film to prevent the ice film from evaporating during the experiment. Additional water vapor from the HONO solution, which was nearly in equilibrium with the vapor pressure of ice, was also introduced to compensate for the ice-film loss from the evacuation.

Because the ice film sublimation rate was substantially higher at 230 K,[19] the loss of the ice film due to evacuation in the flow reactor was noticeable if no additional water vapor was introduced to the reactor. The ice film was difficult to grow at 230 K. For measurements conducted at 230 K, the ice film was vapor deposited at 200 K. The solid ice film was then rapidly warmed to 230 K. Besides the extra ice film and additional water vapor, the total pressure of the reactor was increased to 2.0 Torr, to reduce the loss of the ice film.

HBr−He mixtures. The HBr−He mixture was prepared by mixing HBr (Matheson, 99.8%) and helium (Praxair, scientific grade 99.9995%) in an all-glass manifold, which had been previously evacuated to $\sim 10^{-6}$ Torr. The typical HBr-to-He mixing ratio was between 10^{-3} and 10^{-5}. HBr, along with additional helium carrier gas, was introduced into the flow reactor via the glass and PFA tubing, and the amount was controlled by either a stainless steel flow controller (Teledyne−Hastings) or Monel metering valve. All of the tubings and valves were passivated by the HBr−He mixture to establish equilibrium, as monitored by the QMS prior to every experiment.

HONO Preparation and Calibration. Nitrous acid was prepared by mixing a $NaNO_2$ solution with an H_2SO_4 solution.[20,21] A 2.76 g quantity of $NaNO_2$ (Aldrich) was dissolved in 200 mL of distilled water; a few drops of 40% H_2SO_4 solution were added while the $NaNO_2$ solution was stirred. The acidity of the solution was adjusted to pH 4.0, as monitored by a pH meter (Corning). A colorless, clear HONO solution was obtained. The prepared HONO solution was kept in the dark at 273 K.

Helium carrier gas was bubbled through the HONO solution. Both the HONO vapor and the water vapor from the HONO solution were admitted into the reactor. The HONO vapor at 273 K was measured by an FTIR spectrometer (Mattson, RS-2) with a narrow band MCT detector to ensure the vapor-phase composition. The IR spectra showed a few strong transitions of the N−O stretch at 1700 cm^{-1}, the HON bend at 1263 cm^{-1}, and the O−N stretch at 790 cm^{-1} for the *trans*-HONO isomer. For the *cis*-HONO isomer, the N−O stretch at 1641 cm^{-1}and the O−N stretch at 852 cm^{-1} were observed. All of the absorption frequencies in the IR spectrum agreed with the standard database.[22]

The gas-phase HONO concentration was determined by a long-path IR absorption experiment based on the effective HONO absorption cross-section.[23] BaF_2 windows were used in the IR cell. The partial pressure of HONO near the outlet of HONO bubbler was determined to be 0.019 and 0.013 Torr at 790 and 852 cm^{-1}, respectively. The major gaseous impurities were NO_2 and NO, in addition to H_2O. The NO_2 and NO impurities were approximately 6- and 13-fold higher than that of the HONO concentration, as determined by the infrared absorption.

The HONO vapor pressure above the solution could be, in principle, determined from Henry's law. The concentration of HONO in the solution was calculated from the following equilibrium and Henry's law:

$$NO_2^- + H^+ \rightleftharpoons HONO \tag{1}$$

$$K_a = \frac{[H^+][NO_2^-]}{[HONO]} \tag{2}$$

where $[H^+]$ was determined by the pH meter and $[NO_2^-]$ was the equilibrium concentration of the $NaNO_2$ solutions. Using a dissociation constant, K_a, of 5.6×10^{-4} at 298.15 K and an enthalpy change of eq 1,[24] the gas-phase HONO concentration could be calculated from the following equation.

$$P_{HONO} = \frac{[NO_2^-]_T}{K_H\,(1 + K_a/[H^+])} \tag{3}$$

where K_H is a Henry's law constant. $K_H = 49$ M/atm at 298.15 K and was determined to be 218 M/atm at 273.15 K, based on $d(\ln K_H)/d(1/T) = 4900$.[21,25] $[NO_2^-]_T$ is the initial $NaNO_2$ concentration or total N(III) concentration. We found that the calculated gaseous HONO concentration was more than 2-fold higher than that determined from the IR measurement. The exact reason is unknown to us. One possible cause of this could be a combination of HONO decomposition, the HONO loss on the wall of transfer lines and cell, and perhaps the uncertainties in equilibrium constants.[26] In this paper, we used the mean gaseous HONO concentration determined from the IR absorption because it was closest to our experimental conditions.

In the nitrous acid solutions, HONO might be decomposed by the reactions[5,21,25,27]

$$2\mathrm{HONO} \rightleftharpoons \mathrm{NO_2} + \mathrm{NO} + \mathrm{H_2O} \quad (4)$$

$$2\mathrm{NO_2} + \mathrm{H_2O} \rightleftharpoons \mathrm{HNO_3} + \mathrm{HONO} \quad (5)$$

Gas-phase HONO, NO_2, NO, and water vapor from the HONO solutions were transferred via tubing and admitted into the reactor. We were concerned that HONO might rapidly decompose in the gas phase while being transferred to the reactor. HONO, NO_2, NO, and water vapor were assumed to be in equilibrium over the nitrous acid solutions in the bubbler. The HONO concentration was governed by Henry's law. When the helium gas was bubbled through the HONO solutions, HONO could be decomposed in the transfer lines. We measured the HONO signal using the QMS, after HONO flowed through a 6-in. length of tubing and an 80-in. length of tubing, respectively. There was no noticeable difference in the HONO signal by the QMS at $m/e^- = 47$ between the two cases. This demonstrated that a change in HONO concentration was not detectable during the transfer to the flow reactor under the fast-flow condition. The uncertainty of HONO concentration was estimated to be about 20−30%, as determined by the FTIR. From our measurements, there were no detectable reactions for NO_2 + HBr and NO + HBr over the ice surface at 190 K. The gas-phase reactions between NO_x and HBr were negligibly small.[28]

Determination of the Uptake Coefficient and Reaction Probability. The procedure for the uptake-coefficient measurement was nearly identical to the reaction-probability measurements. We use the reaction probability measurements to illustrate the experimental procedures. The reaction probability γ_w of HONO with HBr on the ice film was determined as follows: First, an ice film was vapor-deposited on the inner wall of the flow reactor. Second, the first section of the film surface (see ice-film preparation section) was pretreated with HBr at pressures between 2.5×10^{-8} and 6.5×10^{-5} Torr for ~10 min. The ice-film surface was not completely saturated by HBr. Finally, HONO was admitted to the reactor with continuing HBr flow in a separated capillary. The gas-phase loss of HONO was measured by the QMS at $m/e^- = 47$ as a function of the injector position z. In all of the experiments, the concentration of HBr was always larger than that of HONO. For a pseudo first-order reaction under the plug-flow condition, the following equation holds for the reactant HONO:

$$\ln[\mathrm{HONO}]_z = -k_s(z/v) + \ln[\mathrm{HONO}]_0 \quad (6)$$

where z is the injector position, v is the mean flow velocity, $[HONO]_z$ is the gas-phase HONO concentration measured by the QMS at position z, and the subscript zero is the initial reference injector position. For a typical experiment performed on the ice film at 190 K, the first-order HONO decay is shown in Figure 1. The pseudo first-order reaction rate constant, k_s, was calculated from the least-squares fit of the experimental data to eq 6. $k_s = 113$ s^{-1} at 190 K was obtained and is shown in the figure. The value of k_s was then corrected for gas-phase axial and radial diffusion using a standard procedure,[29] and the corrected rate constant was called k_w. A diffusion coefficient for HONO in helium was estimated using the Fuller equation, and was expressed as[30]

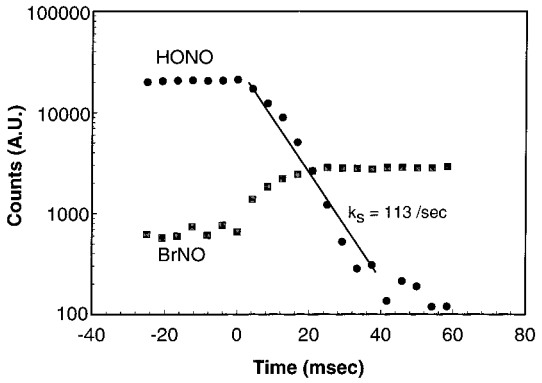

Figure 1. Plot of the HONO signal versus the reaction time (z/v) at 190 K. The pseudo first-order rate constant $k_s = 113$ s^{-1} and the radial and axial diffusion corrected rate constant $k_w = 121$ s^{-1}. The reaction probability $\gamma_w = 6.5 \times 10^{-3}$. A signal for the product BrNO is also shown in the figure.

$$D = 2.3853 \times 10^{-2}\, T^{1.75}/P \quad (7)$$

where T is the temperature in Kelvin and P is the total pressure of the reactor in Torr. The reaction probability γ_w was calculated from k_w using the following equation.

$$\gamma_w = 2R\, k_w /(\omega + R\, k_w) \quad (8)$$

where R is the radius of the flow reactor (0.85 cm) and ω is the mean HONO molecular velocity at the ice-film temperature.

A layered pore-diffusion model was employed to correct the ice-film porosity to obtain the "true" reaction probability γ_t.[31−34] γ_t is equivalent to a reaction probability determined as if the ice film were a "homogeneous" layer over the glass surface. This is useful to model the surface reaction mechanism. On the basis of previous studies conducted under nearly identical conditions,[32,18,34,35] it is known that H_2O ice films can be approximately treated as hexagonally close-packed spherical granules stacked in layers.[32] The "true" reaction probability, γ_t, is related to the value, γ_w, by

$$\gamma_t = \frac{\sqrt{3}\gamma_w}{\pi\{1 + \eta[2(N_L - 1) + (3/2)^{1/2}]\}} \quad (9)$$

where the effectiveness factor η is the fraction of the film surface that participates in the reaction,[32] and N_L is the number of granule layers.[36] Approximately, this model can be considered as the deconvolution of the reaction probability as if the reaction occurred on the top layer of the surface. The detailed calculations for these parameters can be found in ref 32. A tortuosity factor $\tau = 4$ and true ice density $\rho_t = 0.925$ g/cm^3 were used in the above calculation. This was based on a treatment of the ice film that was vapor-deposited on the flow tube at nearly identical conditions.[31,32]

The reaction probability of HONO + HBr can also be determined by the formation of the product BrNO. The reaction product, BrNO, was measured by the QMS at its parent peak

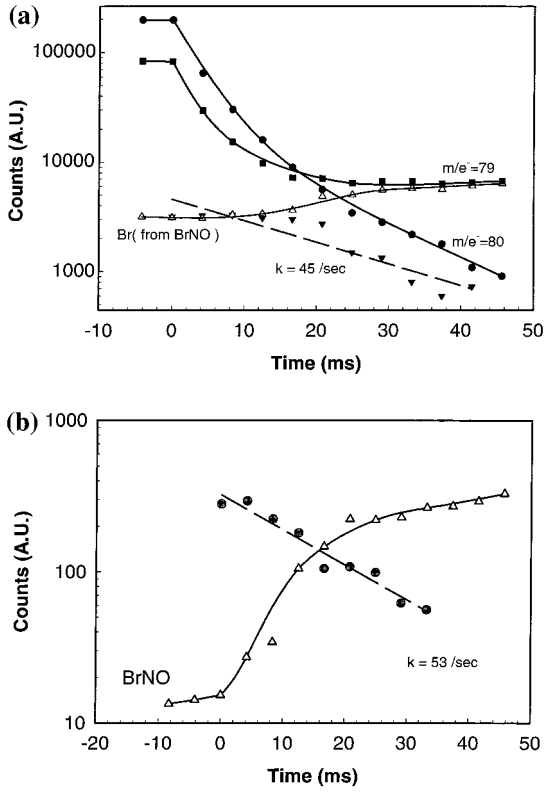

Figure 2. (a) Plot of the fragment Br signal (Δ) ($S_{79} - 0.40S_{80}$) from BrNO versus the reaction time. The signals from $m/e^- = 79$(■) and $m/e^- = 80$ (●) were shown in the figure. The Br fragment signal from BrNO was replotted in the form of ($[BrNO]'_\infty - [BrNO]'_z$), shown as the solid triangles. The pseudo first-order reaction rate constant was calculated from the Br signal using eq 10 to be 45 s^{-1}. (b) Plot of the BrNO signal versus the reaction time. The pseudo first-order reaction rate constant was calculated from this data set to be 53 s^{-1}, which is shown as a dashed line.

$m/e^- = 109$. The increase in the BrNO signal was observed at a high HBr partial pressure (See Figure 1). k_s was calculated from the following equation

$$\ln([BrNO]_\infty - [BrNO]_z) = -k_s(z/v) + \ln[BrNO]_\infty \quad (10)$$

where $[BrNO]_\infty$ was the BrNO concentration when all HONO molecules were converted to BrNO, and $[BrNO]_z$ was the BrNO concentration at the position z. By using BrNO data, k_s was calculated to be 96 s^{-1}, which was very close to the k_s value of 113 s^{-1} determined from the HONO decay data shown in Figure 1.

Because the parent peak signal of BrNO was approximately 13% of the Br fragment in a BrNO mass spectrum,[16] the parent BrNO signal was difficult to detect by the QMS at a lower HBr partial pressure. Instead of monitoring the parent peak BrNO, both $m/e^- = 79$ (Br) and $m/e^- = 80$ (HBr) signals were recorded by the QMS. The difference between the total $m/e^- = 79$ signal and Br fragment signal of HBr was the Br fragment signal present in BrNO molecules. The ratio of the Br fragment signal from the HBr molecule to HBr parent signal was determined to be 40:100 by the QMS using pure HBr at an ionization voltage of 66 eV condition. This ratio is in very good agreement with the literature value of 39:100.[22] Figure 2a illustrates the total $m/e^- = 79$ signal (S_{79}), the HBr signal (S_{80}), and the difference ($S_{79} - 0.40S_{80}$), which was proportional to the concentration of BrNO. $[BrNO]' = (S_{79} - 0.40S_{80})$ was replotted in the form of ($[BrNO]'_\infty - [BrNO]'_z$), and the pseudo first-order reaction rate constant was determined to be 45 s^{-1}.

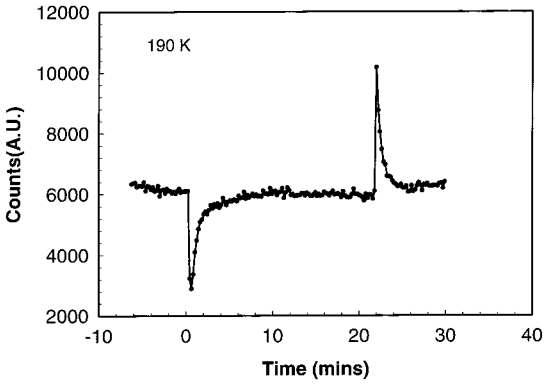

Figure 3. Uptake of HONO on water−ice at $P_{HONO} = 1.9 \times 10^{-7}$ Torr and 190 K. (●) represents the HONO signal. The uptake starts at $t =$ 0 min when the injector was pulled out. The entire ice film (150 cm^2) was saturated within 3 min. Desorption occurred when the injector was pushed in. This procedure can be repeated a few times.

For purposes of comparison, Figure 2b shows the increase of the BrNO signal, based on the direct measurement of the BrNO parent signal. The pseudo first-order reaction rate constant was calculated to be 53 s^{-1}. The two rate constants are in very good agreement. It is important to point out that the HBr surface concentration was assumed to be nearly constant in the calculation of rate constant. This assumption can be justified as the ice film was pretreated by HBr prior to the reaction probability measurement. During the measurement, the loss of HBr to the ice surface was significantly lower than the amount HBr adsorbed on the ice surface. However, one would still observe some gaseous HBr loss, which would not affect the measurements significantly. A sound approach was to saturate the ice surface by HBr. However, this would form hydrate(s) and erupt the HBr-treated ice film.[11,12]

The uptake amount was determined by measuring the total amount of HONO lost onto the ice surface till the surface was saturated as monitored by the QMS. The experimental procedure was identical to our previous study.[11,12,37] The detailed procedures can be found from these references.

Results

Uptake of HONO on Water−Ice. Figure 3 is a plot of the gas-phase HONO signal versus the experimental time for the exposure of HONO on an ice surface. In this experiment, an ice film was deposited on the wall of the flow reactor. The gas-phase HONO signal, as monitored by the QMS at $m/e^- = 47$, decreased rapidly when HONO reached the entire ice surface. The entire ice film was saturated in less than 3 min at 190 K. The uptake amount Θ was determined to be 1×10^{14} molecules/cm^2 at 190 K, based on the geometric surface area of the flow reactor. For cases in which the HONO-saturated ice film was "heated" by the injector (i.e., the injector was pushed back), HONO was desorbed and quantitatively recovered as recorded by the QMS. The uptake amount of HONO was almost identical to the desorbed HONO amount. The uptake and desorption procedure could be repeated several times. The uptake amount of HONO on the ice film was measured at different surface temperatures and is shown in Figure 4. The "heat of uptake" ΔH_{upt} of HONO on ice was determined to be -8.1 ± 2.0 kcal/mol from the slope of a plot of log Θ versus $1/T$ (see Figure 4) using eq 11.

$$\ln \Theta = -\frac{\Delta H}{RT} + C \quad (11)$$

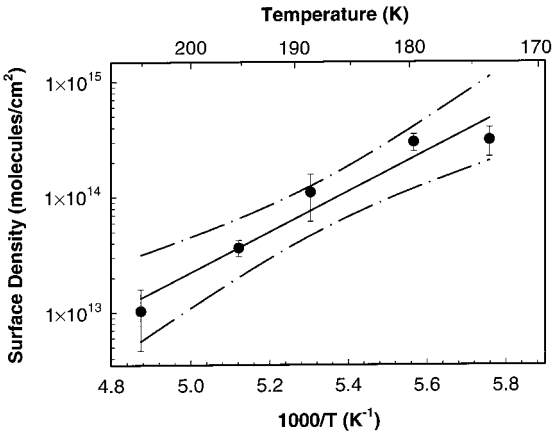

Figure 4. Plot of the logarithm of HONO surface density versus 1/*T*. The solid line is the least-squares fit to the experimental data, and the dashed lines represent the 95% confidence level. The total pressure was 0.50 Torr, $P_{HONO} = 1.9 \times 10^{-7}$ Torr and the film thickness was 30 ± 1 μm. The "heat of uptake" of HONO on ice was -8.1 ± 2.0 kcal/mol.

TABLE 1: Uptake Coefficient of HONO on the Ice Surface between 178 and 200 K[a,b,c]

T (K)	k_s (s^{-1})	k_w (s^{-1})	γ_w	γ_t
178.2	56 ± 6	58	3.7×10^{-3}	1.4×10^{-4}
181.7	43 ± 5	45	2.6×10^{-3}	8.1×10^{-5}
188.9	35 ± 5	37	2.2×10^{-3}	6.4×10^{-5}
192.0	25 ± 4	26	1.6×10^{-3}	3.9×10^{-5}
196.9	14 ± 3	14	8.0×10^{-4}	1.7×10^{-5}
200.2	11 ± 3	11	6.4×10^{-4}	1.3×10^{-5}

[a] $P_{total} = 0.500 \pm 0.02$ Torr. [b] Mean flow velocity $= 15.5 \pm 0.3$ m/s. [c] Ice film thickness $= 30 \pm 1.8$ μm.

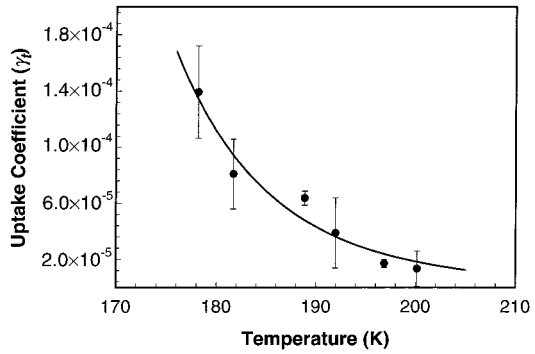

Figure 5. Initial uptake coefficient γ_t of HONO on water−ice at 178 to 200 K. The solid line is the least-squares fit of the experimental data using eq 15.

Uptake Coefficient of HONO on the Ice Film. The uptake coefficient of HONO on the ice film was determined by observing the loss of gas-phase HONO over the ice film surface as a function of the injection position *z*. For every measurement, the ice film was freshly prepared. The measured γ_w represents the initial uptake coefficient. The uptake coefficients were measured as a function of ice-film temperatures, and the results are tabulated in Table 1. The table includes both γ_w and γ_t, and the data were averaged over 2−6 measurements. Data analysis was outlined in the Experimental Section. The "true" uptake coefficient was calculated using eq 9, which was based on the layered pore diffusion model.[32] γ_t as a function of the ice film temperature is shown in Figure 5. Figure 5 shows that γ_t decreased from 1.4×10^{-4} to 1.3×10^{-5} as the temperature increased from 178 K to 200 K. γ_w showed a similar trend as one could read from Table 1. The errors listed in Table 1 and Figure 5 are one standard deviation ($\pm\sigma$) of the mean value. The results indicate that the fraction of HONO molecules sticking on the ice surface is very low. This is consistent with the lower uptake amount at the same temperature range.

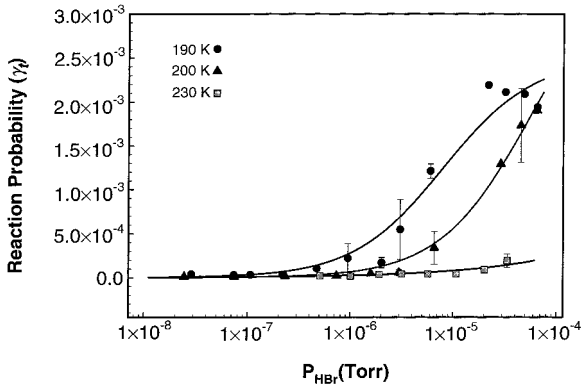

Figure 6. Plot of the "true" reaction probability, γ_t, versus partial HBr pressures for the reaction of HONO + HBr on the ice surface at 190 K (●), 200 K (▲), and 230 K (■). Ice-film thickness was 30 ± 2.2 μm at 190 K, 30 ± 2.5 μm at 200 K, and 33 ± 3.1 μm at 230 K. The solid lines were fitted to eq 21 at 190 and 200 K, and to eq 20 at 230 K.

HONO + HBr → BrNO + H_2O. The reaction probability for the HONO + HBr → BrNO + H_2O reaction was determined by observing the decay of gas-phase HONO over the HBr-treated ice surface as a function of the injection position as shown in Figure 1. In the gas phase, there was no observable reaction between HONO and HBr and between NO_x and HBr. The HONO loss was attributed to the HBr-treated ice surface. The reaction probability γ_w was determined as a function of P_{HBr} and the ice-film temperature. The "true" reaction probability γ_t was calculated by using a layer model in which the ice-film roughness was taken into the consideration.[31,32] The "true" reaction probability γ_t as a function of P_{HBr} at 190 K, 200 K, and 230 K is presented in Figure 6. The detailed experimental conditions, γ_w, and γ_t are listed in Table 2. All data listed in the table were averaged over 2−5 measurements. The errors in Table 2 and Figure 6 represent one standard deviation ($\pm\sigma$) of an average value. The surface concentration of HBr used in this study was always greater than that of HONO, thus the pseudo first-order condition was always satisfied.

Figure 6 shows that the "true" reaction probability γ_t increased from 3.0×10^{-5} to 2.2×10^{-3} at 190 K and from 1.1×10^{-5} to 1.9×10^{-3} at 200 K, as P_{HBr} increased. At a warmer temperature, 230 K, the reaction probability γ_t showed a similar trend, that is, it increased from 1.5×10^{-5} to 1.9×10^{-4} as P_{HBr} increased. However, γ_t is smaller than that of 190 and 200 K.

Table 2 shows that γ_t is ~8- to 50-fold lower than γ_w. At a higher γ_w (i.e., 10^{-2}), the reaction is nearly completed at the external surface before HONO reaches an internal ice surface, and the correction for γ_t is smaller. At a lower γ_w, these HONO molecules, which did not react with adsorbed HBr on the external surface, have an opportunity to diffuse into the internal surfaces and then react with HBr. The pore diffusion model takes this into consideration, and the correction for γ_t is larger.

A reaction product, BrNO, was determined by the QMS using two methods. (1) We took direct measurements, by the QMS, at its parent peak $m/e^- = 109$. The increase of the BrNO signal was observed at 190 K (see Figures 1 and 2b) at a high concentration of HBr. (2) We also took measurements of the Br fragment signal of BrNO. The Br fragment signal was observed to increase during the reaction even at a low concentration of HBr (Figure 2a). Results from both of the

TABLE 2: Reaction Probability for the Reaction of HONO + HBr → BrNO + H_2O on Ice Films between 190 and 230 K[a,b,c,d]

T (K)	P_{HBr} (Torr)	v (m/s)	k_s (s^{-1})	k_w (s^{-1})	$\gamma_{w(HONO)}$	$\gamma_{w(BrNO)}$[e]	$\gamma_{t(HONO)}$
190.9 ± 0.3	2.9×10^{-8}	3.8	26 ± 6	28	$1.6 \pm 0.2 \times 10^{-3}$		3.8×10^{-5}
190.0 ± 1.8	7.4×10^{-8}	3.8	22 ± 5	23	$1.3 \pm 0.3 \times 10^{-3}$	1.1×10^{-3}[f]	3.0×10^{-5}
189.9 ± 1.1	1.1×10^{-7}	3.8	22 ± 6	23	$1.3 \pm 0.4 \times 10^{-3}$	8.7×10^{-4}[f]	3.0×10^{-5}
190.2 ± 0.3	2.2×10^{-7}	15.3	24 ± 3	24	$1.4 \pm 0.1 \times 10^{-3}$	1.5×10^{-3}[f]	3.2×10^{-5}
191.7 ± 0.7	4.7×10^{-7}	15.5	52 ± 5	54	$3.1 \pm 0.3 \times 10^{-3}$	2.6×10^{-3}	1.0×10^{-4}
191.4 ± 1.4	9.5×10^{-7}	15.4	93 ± 45	99	$4.8 \pm 2.7 \times 10^{-3}$		2.2×10^{-4}
191.5 ± 0.7	2.0×10^{-6}	16.2	88 ± 12	92	$4.1 \pm 0.9 \times 10^{-3}$		1.7×10^{-4}
191.3 ± 0.8	3.1×10^{-6}	15.8	128 ± 62	138	$8.0 \pm 3.4 \times 10^{-3}$		5.4×10^{-4}
192.2 ± 1.0	6.0×10^{-6}	16.1	198 ± 30	221	$1.3 \pm 0.4 \times 10^{-2}$		1.2×10^{-3}
192.7 ± 0.8	2.2×10^{-5}	15.8	269 ± 60	314	$1.8 \pm 0.4 \times 10^{-2}$	1.6×10^{-2}	2.2×10^{-3}
191.5 ± 1.2	3.2×10^{-5}	15.6	262 ± 100	307	$1.8 \pm 0.7 \times 10^{-2}$	1.4×10^{-2}	2.1×10^{-3}
192.0 ± 0.3	4.9×10^{-5}	15.6	263 ± 58	306	$1.8 \pm 0.3 \times 10^{-2}$		2.1×10^{-3}
191.2 ± 1.5	6.5×10^{-5}	15.9	255 ± 121	304	$1.7 \pm 0.8 \times 10^{-2}$		1.9×10^{-3}
200.2 ± 0.3	2.5×10^{-8}	3.8	10 ± 7	10	$5.7 \pm 4.0 \times 10^{-4}$		1.1×10^{-5}
199.3 ± 1.2	7.4×10^{-8}	3.8	10 ± 5	10	$5.9 \pm 3.0 \times 10^{-4}$	4.9×10^{-4}[f]	1.1×10^{-5}
200.3 ± 0.3	2.3×10^{-7}	3.8	15 ± 9	15	$8.3 \pm 5.0 \times 10^{-4}$	5.8×10^{-4}[f]	1.7×10^{-5}
199.8 ± 0.5	7.3×10^{-7}	15.3	16 ± 3	16	$9.2 \pm 2.4 \times 10^{-4}$		1.9×10^{-5}
200.5 ± 0.3	1.6×10^{-6}	15.5	31 ± 5	32	$1.8 \pm 0.2 \times 10^{-3}$		4.5×10^{-5}
200.4 ± 0.3	3.0×10^{-6}	15.4	34 ± 11	36	$2.1 \pm 1.0 \times 10^{-3}$		5.5×10^{-5}
200.7 ± 1.5	6.6×10^{-6}	15.7	116 ± 42	127	$6.1 \pm 2.2 \times 10^{-3}$		3.4×10^{-4}
200.0 ± 0.3	2.9×10^{-5}	16.0	205 ± 32	232	$1.3 \pm 0.4 \times 10^{-2}$	1.2×10^{-2}	1.3×10^{-3}
199.8 ± 0.3	4.5×10^{-5}	15.6	251 ± 31	295	$1.6 \pm 0.2 \times 10^{-2}$	1.1×10^{-2}	1.7×10^{-3}
199.7 ± 0.4	6.5×10^{-5}	15.7	255 ± 112	303	$1.6 \pm 0.7 \times 10^{-2}$		1.9×10^{-3}
229.8 ± 0.3	5.1×10^{-7}	9.7	16 ± 3	17	$8.7 \pm 1.6 \times 10^{-4}$		1.7×10^{-5}
229.2 ± 0.3	1.0×10^{-6}	9.9	15 ± 5	15	$7.6 \pm 3.0 \times 10^{-4}$		1.5×10^{-5}
230.0 ± 0.3	1.9×10^{-6}	10.2	28 ± 21	29	$1.5 \pm 0.9 \times 10^{-3}$		3.4×10^{-5}
229.6 ± 0.3	3.2×10^{-6}	10.6	31 ± 10	32	$1.7 \pm 0.3 \times 10^{-3}$		3.9×10^{-5}
228.3 ± 0.3	5.7×10^{-6}	10.0	30 ± 9	31	$1.6 \pm 1.3 \times 10^{-3}$		3.8×10^{-5}
230.2 ± 0.5	1.1×10^{-5}	9.9	32 ± 12	33	$1.7 \pm 0.5 \times 10^{-3}$		4.1×10^{-5}
229.2 ± 0.8	2.0×10^{-5}	10.3	52 ± 9	54	$2.8 \pm 0.4 \times 10^{-3}$		8.8×10^{-5}
229.4 ± 0.8	3.4×10^{-5}	10.6	79 ± 24	85	$4.5 \pm 1.1 \times 10^{-3}$		1.9×10^{-4}

[a] The total pressure was 0.501 ± 0.01 Torr at 190 and 200 K (except $P_{HBr} < 2 \times 10^{-7}$ Torr, where the total pressure was 2.00 ± 0.02 Torr). [b] The total pressure was 2.00 ± 0.02 Torr at 230 K. [c] Ice film thickness was 30 ± 2.2 μm, 30 ± 2.5 μm, and 33 ± 3.1 μm at 190, 200, and 230 K, respectively. [d] $P_{HONO} = (1.9 \pm 1.0) \times 10^{-7}$ Torr with the exception of when P_{HBr} is less than 7×10^{-7} Torr where $P_{HONO} = (1.1 \pm 0.9) \times 10^{-8}$ Torr. [e] $\gamma_{w(BrNO)}$ was calculated from the BrNO signal. [f] Means that $\gamma_{w(BrNO)}$ was calculated from the Br fragment signal of the BrNO molecule. (See text for details.)

methods indicated that BrNO was formed during the reaction, and that the measured reaction probabilities were consistent with each other, as shown both in Figure 2 and in Table 2.

IV. Discussion

1. Uptake of HONO on Ice Film. Figure 3 showed the HONO loss on the ice surface as a function of the time. The HONO loss rate onto the ice surface was approximately constant at $t \approx 0-0.5$ min and then decreased nonlinearly until it reached saturation coverage. This suggested that the uptake coefficient varied slightly at the lower coverage and then decreased to zero at saturation coverage. This trend cannot be explained by assuming that the adsorbate binds to a series of identical surface sites, which predicts that the uptake coefficient varies linearly with the coverage.[38]

The behavior of the HONO loss on the ice surfaces may be explained by the following: A gas-phase HONO molecule impinges on an occupied site that could not be adsorbed. However, the molecule could be trapped into a weakly bound state. The molecule can then diffuse around the surface and find a site to adsorb. This can be summarized by the following equations:

$$\mathrm{HONO(g)} \underset{k_2}{\overset{k_1}{\rightleftharpoons}} \mathrm{HONO(p)} \qquad (12)$$

$$\mathrm{HONO(p)} \xrightarrow{k_3} \mathrm{HONO(ad)} \qquad (13)$$

Reaction 12 represents the gas-phase HONO molecules entering and desorbing out of the weakly bound state. Reaction 13 represents the migration of HONO from the weakly bound state to the adsorption site. From 178 to 200 K, the uptake amount of HONO on the ice surface is relatively low, approximately 1×10^{14} molecules/cm^2. This agrees with the idea that HONO molecules trap onto a weakly bound state and also desorb to the gas phase because of thermal energy. With the suggestion of a lower γ_t or γ_w, a small fraction of HONO molecules are able to move to the adsorption state between 178 and 200 K. This fraction of molecules may control the uptake rate, and it is reasonable to assume that the initial uptake coefficient is limited by the rate of reaction 13. This can be expressed as

$$\mathrm{Rate} = k_3[\mathrm{HONO(p)}] \qquad (14)$$

[HONO(p)] can be calculated from reaction 12 using the steady-state approximation. The uptake coefficient can be written in terms of eq 14 as follows:

$$\gamma_t = \frac{\mathrm{Rate}}{(1/4)[\mathrm{HONO(g)}]\omega(A/V)} = \frac{\alpha}{k_2/k_3} = \frac{\alpha}{\nu_2/\nu_3 \exp(-(E_2 - E_3)/k_B T)} \qquad (15)$$

where ω is the molecular velocity of HONO, A/V is the surface-to-volume ratio, $\alpha = 4k_1V/\omega A$, ν_i is the preexponential factor, and k_B is the Boltzmann constant. The "true" uptake coefficients were fitted to eq 15, and the result is shown in Figure 5 as a solid line. This line fit the experimental data very well from 178 to 200 K. $E_2 - E_3 = 6.5$ kcal/mol was obtained from the least-squares fit. E_2 is the activation energy of molecules from the weakly bound state to the gas phase. E_3 is the activation

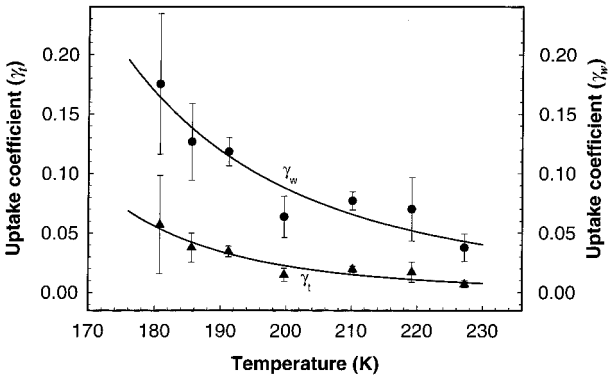

Figure 7. Initial uptake coefficient of HBr on water−ice between 181 and 227 K. The total pressure was 0.50 Torr, $P_{HBr} = 1.0 \times 10^{-6}$ Torr, and the film thickness was 28 ± 2.1 μm. (●) was the uptake coefficient γ_w of HBr on water−ice. (▲) was the "true" uptake coefficient γ_t of HBr on water−ice as corrected by the pore diffusion model. See details in the text.

energy of molecules from the weakly bound state to the adsorption state. $E_2 - E_3 = 6.5$ kcal/mol indicates the barrier between the weakly bound state and the adsorption state. The relatively high barrier is reflected in the small uptake amount and lower uptake coefficient. We may compare this $E_2 - E_3$ value to a few similar systems. $E_2 - E_3 = 4.1$ kcal/mol for $ClONO_2$ hydrolysis on the ice surface and 5.6 kcal/mol for the HOBr uptake on the ice surface.[39,40] These values are slightly lower than $E_2 - E_3$ of HONO/ice and, thus, have higher uptake coefficients.

2. HONO + HBr Reaction. First, we will examine some experimental observations for HBr and HONO on the ice surface and then draw some conclusions about the reaction mechanism.

A. HBr on Ice. The initial "true" uptake coefficient γ_t of HBr on pure ice varied from 0.06 to 0.007 for cases in which the temperature increased from 181 to 227 K, as shown in Figure 7. The solid lines in Figure 7 are used to guide the reader's eye. γ_w is also shown in Figure 7 in the same scale. It is clear that γ_t at 230 K is smaller than those found between 190 and 200 K. It is important to note that the HBr uptake coefficient is higher than the reaction probability of HONO + HBr at the same temperature and P_{HBr}. The desorption temperature of HBr was ~225−230 K for $P_{HBr} = 1 \times 10^{-6}$ Torr, and the total pressure of the flow reactor was 0.5 Torr.[14] This suggested that HBr adsorbed on the ice surface during the reaction.

B. HONO on Ice. Figures 3 and 4 indicated that the HONO uptake rate by the ice surface was low, and HONO was easy to desorb by the warm (about 10 degree higher) injector. By comparing the "heat of uptake", ΔH_{upt}, of HONO to ΔH_{upt} of HOCl on ice, we hope to draw some conclusions about the interaction between HONO and water. The desorption temperature of HOCl on ice is between ~170−175 K.[41,42] The mean "heat of uptake" of HOCl on the ice surface was -10 ± 2 kcal/mol.[43] ΔH_{upt} of HONO on ice (-8.1 ± 2.0 kcal/mol) is slightly lower than that of HOCl. This indicates that the interaction between HONO and ice was weaker than that of HOCl with ice. We expect that the desorption temperature of HONO on ice is likely lower than 175 K. The surface residence time τ of HONO on ice at 190 and 200 K can be estimated from ΔH_{upt} on the basis of $\tau = \tau_o \exp(-\Delta H_{upt}/k_B T)$ to be about milliseconds. This indicates that the chance for HONO molecules to desorb is fairly high, at 190 K or higher.

C. Reaction Mechanism. On the basis of the above analysis, HBr is adsorbed on the ice surface and HONO is mainly in the gas phase between 190 and 230 K. A possible mechanism is proposed by the following reactions:

$$HBr(g) + 2S \underset{k_2}{\overset{k_1}{\rightleftharpoons}} HBr(ad) \leftrightarrow H^+(H_2O)(ad) + Br^-(H_2O)(ad) \quad (16)$$

$$Br^-(ad) + HONO \xrightarrow{H^+} HONO\cdots Br^-(ad) \xrightarrow[H^+]{k_s} BrNO(g) + H_2O(ad) \quad (17)$$

We expect that reaction 17 is the rate-determining step. The reasons are as follows: The initial uptake coefficient of HBr on the ice surface ($\gamma_w = 0.12$ at 190 K, $P_{HBr} = 1.0 \times 10^{-6}$ Torr) is always higher than the reaction probability of HONO + HBr reaction ($\gamma_w = 0.0048$ at 190 K, $P_{HBr} = 1.0 \times 10^{-6}$ Torr). HBr was in excess and HONO was the limiting agent in this study. This suggests that reaction 16 cannot be the rate-limiting step. The rate of the reaction is proportional to the HBr surface concentration, and the partial pressure of HONO, P_{HONO}

$$R = -\frac{d[\mathrm{HONO}]}{dt} = k_s [HBr]_{ad} P_{HONO} \quad (18)$$

The HBr surface concentration in eq 18 can be derived from the steady-state approximation and adsorption equilibrium of eq 16.

$$[\mathrm{HBr}]_{(ad)} = [\mathrm{Br}^-]_{(ad)} = \left(\frac{k_1}{k_2}\right)^{1/2} P_{HBr}^{1/2} S = b_{HBr} P_{HBr}^{1/2} S \quad (19)$$

where $b_{HBr} = (k_1/k_2)^{1/2}$, $S_o = S + [\mathrm{Br}^-]_{ad} + [\mathrm{H}^+]_{ad} = S + 2[\mathrm{HBr}]_{ad}$, and S_o and S are the total number of sites on the surface and available site, respectively.

Reaction probability, γ, is given by $R/(\phi_{HONO}\, A/V)$, where ϕ_{HONO} is the total HONO flux colliding on the surface ($\phi_{HONO} = P_{HONO}/\sqrt{2\pi m k_B T}$, where m is the molecular weight of HONO), A/V is the surface-to-volume ratio, and is expressed by eq 20

$$\gamma_t = \frac{R}{\phi_{HONO}(A/V)} = \frac{c b_{HBr} k_s P_{HBr}^{1/2} S_0}{1 + 2 b_{HBr} P_{HBr}^{1/2}} \left(\frac{V}{A}\right) = \gamma_o \frac{b_{HBr} P_{HBr}^{1/2}}{1 + 2 b_{HBr} P_{HBr}^{1/2}} \quad (20)$$

where $c = \sqrt{2\pi m k_B T}$, $\gamma_0 = c(V/A)\, k_s\, S_o$, and b_{HBr} is a constant at a given temperature. The term $b_{HBr} P_{HBr}^{1/2}$ represents the HBr molecules dissociatively adsorbed on the ice surface based on eq 16.

For the experimental data at 190 K, the fitted result by using eq 20 is shown in Figure 8 as the dashed line. Apparently, the data were not well fitted. When HBr adsorbed on the ice surface between 190 and 200 K, hydrates were likely to be formed near the ice surface.[11] Previously, we have shown the isotherms for HBr on the ice surface can be written as $\theta = K P^f$, where $f = 0.83$.[11,12] In terms of a mathematical expression of the isotherms, this is close to the Langmuir isotherm. If we allow HBr to form hydrate(s), the expression for $[\mathrm{HBr}]_{ad}$ in eq 20 must change. We can write eq 20 as

$$\gamma_t = \frac{R}{\phi_{HONO}(A/V)} = \frac{\frac{c k_1 k_s}{k_2} P_{HBr} S_0}{1 + \frac{k_1}{k_2} P_{HBr}} \left(\frac{V}{A}\right) = \gamma_o \frac{b_{HBr} P_{HBr}}{1 + b_{HBr} P_{HBr}} \quad (21)$$

where we approximately treated the hydrate(s) as associative forms, and the Langmuir isotherm was used. The chemical

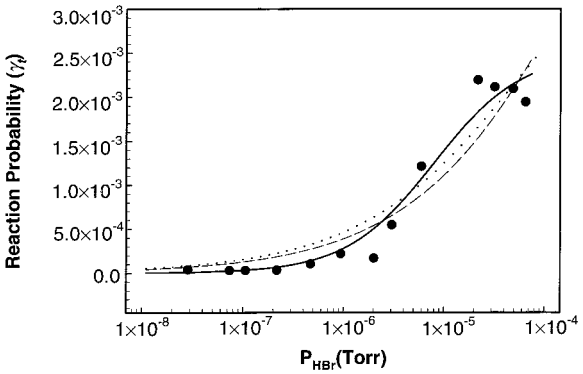

Figure 8. Plot of the reaction probability, γ_t, versus partial HBr pressures for the reaction of HONO + HBr on the ice surface at 190 K (●). The solid line was fitted to eq 21, and the dashed line was fitted to eq 20 for Eley−Rideal mechanism. The dotted line was fitted to eq 22 if the reaction follows Langmuir−Hinshelwood mechanism. (See text for details.)

nature for HBr•nH$_2$O is ionic within the molecular crystal. The experimental data at 190 K were fitted by eq 21, and the result is shown in Figure 8 as a solid line, which fit the experimental data very well. Both solid lines at 190 and 200 K in Figure 6 were fitted by eq 21. However, for cases in which the data at 230 K were fitted to eq 21, the result was unsatisfactory. The experimental data at 230 K could be fitted by eq 20 very well, and the result is shown in Figure 6 as the solid line. The conclusion drawn from this exercise is that at 190 and 200 K, HBr may form hydrates, and the hydrate is adsorbed near the ice surface. The adsorbed HBr reacts with incoming HONO molecules via the Eley−Rideal mechanism to form BrNO, which subsequently desorbs from the surface. The analysis showed that HBr behaves like a dissociative adsorption on the ice surface at 230 K. We speculate that either HBr is dissociatively adsorbed on the ice surface or HBr is in a quasi-liquid layer that results in a higher ion mobility for $H^+(H_2O)_n$ and Br^-. This suggestion is supported by the HBr−ice-phase diagram at the low temperature,[12] in which HBr is either in the metastable "ice" phase or in the liquid phase, depending on the partial HBr pressure. Both states are believed to have free ions, namely Br^- and $H^+(H_2O)$. In terms of the isotherm, it behaves just like a dissociative adsorption and has the functional form of eq 20.

The above discussion was based on the experimental fact that HONO was unlikely to be adsorbed on the ice surface at 190 K and above. If we assume that both HONO and HBr were adsorbed on the ice between 190 and 230 K, the reaction follows a Langmuir−Hinshelwood mechanism. The reaction probability can be expressed as

$$\gamma_t = \gamma_o \frac{b_{HONO} b_{HBr} P_{HBr}^{1/2}}{(1 + 2b_{HBr} P_{HBr}^{1/2} + b_{HONO} P_{HONO})^2} \qquad (22)$$

where b_{HONO} is an adsorption constant. An attempt was made to fit the experimental data at 190 K by eq 22 at a constant P_{HONO} condition, and the result is shown in Figure 8 as the dotted line. Clearly, it does not represent the experimental data very well. This evidence further indicates that the reaction is not likely to be Langmuir−Hinshelwood type.

D. Effect of the Temperature on the Reaction Probability. The reaction probability decreases as the temperature increases. The reaction probabilities at 190 and 200 K are similar, but the reaction probability at 230 K is lower than that of 190 and 200 K. This may be attributed to the fact that the desorption of HBr on ice occurs between ∼225−230 K in the fast-flow reactor.[14] This implies that the surface residence time of HBr is reduced dramatically above the desorption temperature, and thus, the adsorbed HBr amount is reduced (i.e., increased k_2 in eq 16 or decreased b_{HBr}). HBr is not readily available for the reaction. A reduction in the reaction rate is expected near the desorption temperature and above.

3. Comparison to Previous Study. For HONO uptake on the ice surface, Fenter and Rossi reported that the uptake coefficient γ_w of HONO was 1×10^{-3} at 180 K.[44] We determined that the uptake coefficient, γ_w, of HONO on water−ice was 2.3×10^{-3} at 180 K. Within the uncertainties of measurement, this study is in very good agreement with the earlier study.

The uptake amount of HONO was not studied previously. The uptake amount of HONO was determined to be between 3×10^{14} and 1×10^{13} molecules/cm^2 between 173 and 205 K in this study. It is close to the uptake amount of HOCl, between 1×10^{14} and 5×10^{13} molecules/cm^2 between 189 and 220 K.[14]

Seisel and Rossi reported that the average uptake coefficient γ_w of HBr on ice was 0.32 ± 0.12 between 180 and 200 K and showed a slightly negative temperature dependence from 180 to 200 K.[16] Flückiger et al. reported a value between 0.2−0.34 from 190 to 210 K.[45] Hanson and Ravishankara reported the uptake coefficient was larger than 0.2 at 200 K.[46] This study determined the initial uptake coefficient γ_w to be between 0.17 and 0.04, which decreased as the temperature increased from 181 to 227K. The results of this study are slightly lower than previous reports, but they show the same trend of the negative temperature dependence. Within the uncertainties of the experiments, we would consider our results in agreement with previous results.

For the reaction HONO + HBr → BrNO + H$_2$O, we may compare our study to the previous measurement. Seisel and Rossi reported that the reaction probability γ_w was 8.8×10^{-3} - 2.2×10^{-2} at 180 K, 1.7×10^{-4} - 2.2×10^{-2} at 190 K, and 1.3×10^{-3} - 9.7×10^{-3} at 200 K.[16] Our results suggest that γ_w is between 1.3×10^{-3} and 1.8×10^{-2} at 190 K and between 5.7×10^{-4} and 1.6×10^{-2} at 200 K. Within the uncertainties of the measurement, this study is in excellent agreement with the earlier study.

4. Atmospheric Implications. The heterogeneous formation of photochemically active BrNO may play a role in the partitioning of bromine compounds in the lower stratosphere and in the troposphere. This study indicates that the bromine-activation efficiency depends on the HBr concentration and aerosol temperatures. The typical HBr concentration in the stratosphere is ∼2pptv,[47] which is ∼50-fold lower than the HBr concentration used in our measurements. We expect that the reaction probability, γ_w, for the HONO + HBr reaction would be approximately 10^{-3}. If we compare this reaction to some important heterogeneous atmospheric processes with higher reaction probabilities, e.g., $\gamma_w = 0.3$,[48] it is easily concluded that bromine activation via the HONO + HBr is not a critical process in the lower stratosphere. However, a small fraction of BrNO can be formed in the dark night or polar winter time over the PSC surfaces. This will change the bromine partitioning in the lower stratosphere slightly.

At the simulated polar tropospheric temperature of 230 K, the reaction probability γ_w is estimated at $\sim 10^{-4}$. The photolysis rate of HBr at the Arctic ground level is $< 10^{-9}$.[8] HBr is a good reservoir compound in the troposphere. With the 70 pptv HONO concentration in the Arctic,[4] we can speculate that this reaction

may occur over Arctic snow/ice surfaces. If we assume the photolysis rate of BrNO is similar to that of ClNO in the troposphere, the photochemical lifetime of BrNO is on the order of 1 h. This is a potential pathway to activate HBr in the troposphere and may contribute to an understanding of the Arctic boundary ozone loss.[49]

V. Conclusion

This study shows that HONO is rapidly saturated on the water−ice surface between 173 and 230 K. The "true" uptake coefficient of HONO on ice film was determined to be between 1.4×10^{-4} and 1.3×10^{-5} from 178 to 200 K. The "heat of uptake" of HONO on ice was determined to be approximately -8.1 ± 2.0 kcal/mol. The reaction probability of HONO over the HBr treated ice surface increases as P_{HBr} increases over 190−230 K. Kinetic analysis indicated that the heterogeneous reaction of HONO with HBr on ice surfaces followed the Eley−Rideal type.

Acknowledgment. The authors would like to thank Professor Barbara Finlayson-Pitts, who provided the infrared absorption cross section data of HONO and a preprint of reference 23, and two anonymous reviewers for helpful suggestions. The authors also acknowledge financial support by the National Science Foundation under Grant No. ATM-9530659.

References and Notes

(1) Calvert J. G.; Yarwood, G.; Dunker, A. M. *Res. Chem. Intermed.* **1994**, *20*, 463.
(2) Lammel, G.; Cape, J. N. *Chem. Soc. Rev.* **1996**, *25*, 361.
(3) Appel, B. R.; Winer, A. M.; Tokiwa, Y.; Biermann, H. W. *Atmos. Environ.* **1990**, *24A*, 611.
(4) Li, S.-M. *J. Geophys. Res.* **1994**, *99*, 25 469.
(5) Vecera Z.; Dasgupta P. K. *Environ. Sci. Technol.* **1991**, *25*, 255.
(6) McElroy, M.B.; Salawitch, R. J.; Wofsy, S. C.; Logan, J. A. *Nature*, **1986**, *321*, 759.
(7) Lary, D. J. *J. Geophys. Res.* **1996**, *101*, 1505.
(8) Yung, Y. L.; Pinto, J. P.; Watson, R. T.; Sander, S. P. *J. Atmos. Sci*. **1980**, *37*, 339.
(9) Lary, D. J.; Chipperfield, M. P.; Toumi, R.; Lenton, T. *J. Geophys. Res*. **1996**, *101*, 1489.
(10) Abbatt, J. P. D. *Geophys. Res. Lett.* **1994**, *21*, 665.
(11) Chu, L. T.; Heron, J. W. *Geophys. Res. Lett.* **1995**, *22*, 3211.
(12) Chu, L. T.; Chu, L. *J. Phys. Chem. A* **1999**, *103*, 384.
(13) Hanson, D. R.; Ravishankara, A. R. *J. Phys. Chem*. **1992**, *96*, 9441.
(14) Chu, L.; Chu, L. T. *J. Phys. Chem. A* **1999**, *103*, 691.
(15) Allanic, A.; Oppliger, R.; Rossi, M. J. *J. Geophys. Res.* **1997**, *102*, 23 529.
(16) Seisel, S.; Rossi, M. J. *Ber. Bunsen-Ges. Phys. Chem.* **1997**, *101*, 943.
(17) Chu, L. T. *J. Vac. Sci. Technol., A* **1997**, *15*, 201.
(18) Keyser, L. F.; Leu, M.-T. *J. Colloid Interface Sci.* **1993**, *155*, 137.
(19) Haynes, D. R.; Tro, N. J.; George, S. M. *J. Phys. Chem*. **1992**, *96*, 8502.
(20) Zhang, R.; Leu, M.-T.; Keyser L. F. *J. Phys. Chem*. **1996**, *100*, 339.
(21) Park, J.-Y.; Lee, Y.-N. *J. Phys. Chem.* **1988**, *92*, 6294.
(22) NIST Standard Reference Database Number 69. http://webbook.nist.gov/chemistry/, November 1998 Release.
(23) Barney, W. S.; Wingen, L. M.; Lakin, M. J.; Brauers, T.; Stutz, J.; Finlayson-Pitts, B. J. *J. Phys. Chem. A* **2000**, *104*, 1692.
(24) Lide, D. R. *CRC Handbook of Chemistry and Physics*, 78th edition; CRC Press: New York, 1998; pp 8−44.
(25) Becker, K. H.; Kleffmann, J.; Kurtenbach, R.; Wiesen, P. *J. Phys. Chem.* A **1996**, *100*, 14 984.
(26) Becker, K. H.; Kleffmann, J.; Kurtenbach, R.; Wiesen, P.; Febo, A.; Gherarhi, M.; Sparapani, R. *Geophys. Res. Lett*. **1995**, *22*, 2485.
(27) Wiesen, P.; Kleffmann, J.; Kurtenbach R.; Becker K. H. *Faraday Discuss*. **1995**, *100*, 121.
(28) Rosser, W. A., Jr.; Wise, H. *J. Phys. Chem.* **1960**, *64*, 602.
(29) Brown, R. L. *J. Res. Natl. Bur. Stand. (U. S.)* **1978**, *83*, 1.
(30) Cussler, E. L. *Diffusion, Mass Transfer in Fluid Systems*; Cambridge University Press: New York, 1984; Chapter 5.
(31) Keyser, L. F.; Moore, S. B.; Leu, M.-T. *J. Phys. Chem*. **1991**, *95*, 5496.
(32) Keyser, L. F.; Leu, M.-T.; Moore, S. B. *J. Phys. Chem*. **1993**, *97*, 2800.
(33) Chu, L. T.; Leu, M.-T.; Keyser, L. F. *J. Phys. Chem.* **1993**, *97*, 7779.
(34) Chu, L. T.; Leu, M.-T.; Keyser, L. F. *J. Phys. Chem*. **1993**, *97*, 12 798.
(35) Keyser, L. F.; Leu, M.-T. *Micros. Res. Tech.* **1993**, *25*, 343.
(36) $N_L = a\,x^b + N \log(x + c)$ where $a = -0.1037$, $b = 4.6841 \times 10^{-15}$, $N = 10.6290$, and $c = 0.8690$. x (= 0.5−35) is the film thickness in μm. The parameters were derived from references 32 and 33. This expression is valid for a thin ice film at about 200 K.
(37) Chu, L. T.; Chu, L. *J. Phys. Chem. B* **1997**, *101*, 6271.
(38) Masel, R. I. *Principles of Adsorption and Reaction on Solid Surfaces*; Wiley: New York, 1996, Chapters 5 and 7.
(39) Berland, B. S.; Tolbert, M. A.; George, S. M. *J. Phys. Chem. A* **1997**, *101*, 9954.
(40) Chu, L.; Chu, L. T. *J. Phys. Chem. A* **1999**, *103*, 8640.
(41) Oppliger, R.; Allanic, A.; Rossi, M. J. *J. Phys. Chem.* **1997**, *101*, 1903.
(42) Bahnam, S. F.; Horn, A. B.; Koch, T. G.; Sodeau, J. R. *Faraday Discuss*. **1995**, *100*, 321.
(43) Calculated on the basis of the results presented in reference 14. Hanson, D. R.; Ravishankara, A. R., *J. Phys. Chem*. **1992**, *96*, 2628. Abbatt, J. P. D.; Molina, M. J. *Geophys. Res. Lett*. **1992**, *19*, 461. Brown, A. R.; Doren, D. J. *J. Phys. Chem. B.* **1997**, *101*, 6308. Geoger, F. M.; Hicks, J. M.; Dios, A. C. *J. Phys. Chem. A* **1998**, *102*, 1514.
(44) Fenter, F. F.; Rossi, M. J. *J. Phys. Chem.* **1996**, *100*, 13765.
(45) Flückiger, B.; Thielmann, A.; Gutzwiller, L.; Rossi, M. J. *Ber. Bunsen-Ges. Phys. Chem*. **1998**, *102*, 915.
(46) Hanson, D. R.; Ravishankara, A. R. In *The Tropospheric Chemistry of Ozone in the Polar Regions*; Niki, H., Becker, K. H., Eds.; NATO ASI Series; Verlag: NY.; 1993, pp 281−290.
(47) Johnson, D. G.; Traub, W. A.; Chance, K. V.; Jucks, K. W. *Geophys. Res. Lett.* **1995**, *22*, 1373.
(48) DeMore, W. B.; Sander, S. P.; Golden, D. M.; Hampson, R. F.; Kurylo, M. J.; Howard, C. J.; Ravishankara, A. R.; Kolb, C. E.; Molina, M. J. *Chemical Kinetics and Photochemical Data for Use in Stratospheric Modeling, Evaulation 12*; JPL: Pasadena, 1997; p 233.
(49) Barrie, L, A.; Bottenheim, J. W.; Schnell, R. C.; Crutzen, P. J.; Rasmussen, R. A. *Nature* **1988**, *334*, 138.